Molecular dynamics study of the interaction between PACAP (6'–38') and the N-terminal extracellular domain of the human splice variant hPAC1-R-short, aiming at the development of neuropathic pain medicine

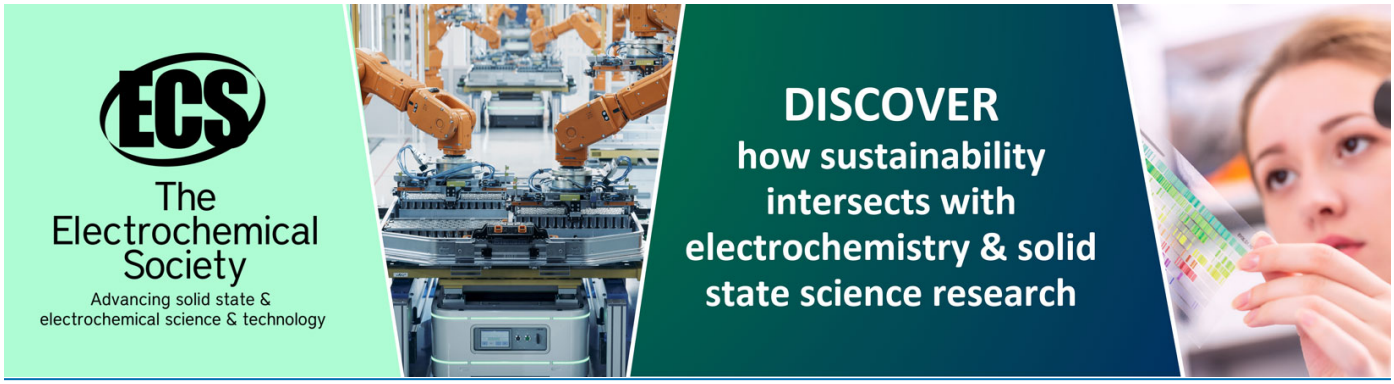

IOP Conf. Series: Journal of Physics: Conf. Series **1136** (2018) 012024 doi:10.1088/1742-6596/1136/1/012024

Molecular dynamics study of the interaction between PACAP (6'–38') and the N-terminal extracellular domain of the human splice variant hPAC1-R-short, aiming at the development of neuropathic pain medicine

Y Watanabe[1,2] A Oda[2,3,4] and H Gouda[1*]

[1]School of Pharmacy, Showa University, 1-5-8 Hatanodai, Shinagawa-ku, Tokyo 142-8555, Japan
[2]Faculty of Pharmacy, Institute of Medical, Pharmaceutial and Health Science, Kanazawa University, Kakuma, Kanazawa, Ishikawa 920-1192, Japan
[3]Graduate School of Pharmacy, Meijo University, 150 Yagotoyama, Tempaku-ku, Nagoya, Aichi 468-8503, Japan
[4]Institute for Protein Research, Osaka University, 3-2 Yamadaoka, Suita, Osaka 565-0871, Japan

[*]E-mail: godah@pharm.showa-u.ac.jp

Abstract. Chronic pathetic pain is caused by an external injury to the peripheral and central nervous systems. The pathogenic mechanism has not been elucidated and existing analgesics are insufficiently effective for pain relief. In the nervous conduction of pain, pituitary adenylate cyclase-activating polypeptide (PACAP), which is constituted by 38 or 27 amino acid residues, acts as a neurotransmitter. Therefore, the selective receptor, namely pituitary adenylate cyclase-activating polypeptide type I receptor (PAC1-R), is a potential target for alleviating neuropathic pain. Detailed investigation on the interaction between PACAP (6'–38') and PAC1-R would be informative for structure-based drug design of the PAC1-R inhibitor because the short analog PACAP (6'–38') acts as a potent antagonist. In this study, we conducted molecular dynamics simulations to investigate the solution structure of the complex of PACAP (6'–38') and the N-terminal extracellular domain of human splice variant hPAC1-R-short (hPAC1-RS). As a result, several strong hydrogen bonds were observed between acidic residues of hPAC1-RS and basic residues of PACAP (6'–38'), which suggests that these residues are important for peptide binding and ligand selectivity.

1. Introduction

Chronic pathetic pain is defined as a prolonged or recurrent pain that persists long after the usual response time to an acute disease, which is represented by an intractable neurogenic disorder such as postherpetic neuralgia or sciatica [1]. Although the onset of chronic pathetic pain is hypothesized to be caused by an external injury to the central and peripheral nerves [1], the pathogenic mechanism of chronic neuropathy has not been elucidated and existing analgesics such as non-steroidal anti-inflammatory agents are insufficiently effective for pain relief. In the nervous conduction of pain, pituitary adenylate cyclase-activating polypeptide (PACAP), which is constituted by 38 or 27 amino acid residues, and vasoactive intimal peptide (VIP), which consists of 28 residues, act as a

neurotransmitter, or nerve modulation factor. PACAP and VIP are known to be important for neuroprotection, neurotrophy and nerve growth [2,3]. PACAP and VIP are bound to the following two subtypes of the Class II G-protein-coupled receptors (GPCR) [4]: subtype I and subtype II. Although the affinity of the subtype II receptor for PACAP is similar to that of VIP, the subtype I receptor selectively binds to PACAP over VIP, with a difference in affinity of more than 1,000-fold [5]. The subtype I PACAP selective receptor, namely the pituitary adenylate cyclase-activating polypeptide type I receptor (PAC1-R), is expressed in the central and peripheral nervous systems and has been suggested as a potential target for the treatment of neuropathic pain [2]. Inhibition of the interaction between PACAP and PAC1-R is expected to reduce neuropathic pain and lead to the development of a new strong painkiller.

Recently, the NMR structure of PACAP (6'–38') in complex with the N-terminal extracellular (EC) domain of the human splice variant hPAC1-R-short (hPAC1-RS) was reported [6]. PACAP (6'–38') is a shorter analog of PACAP-38 and is reported to act as a potent antagonist with a similar affinity to that of a PACAP-38. Therefore, detailed investigation of the interaction between PACAP (6'–38') and the N-terminal EC domain of hPAC1-RS would be informative for structure-based drug design of the PAC1-R inhibitor. In this study, we conducted a molecular dynamics (MD) simulation to investigate the solution structure of the complex of PACAP (6'–38') and the N-terminal EC domain of hPAC1-RS. Using the MD trajectory, the interaction between PACAP and PAC1-R was studied to identify the key residues that are responsible for the strong binding, which would be useful in designing the PAC1-R inhibitor [7]. Moreover, we conducted additional MD simulations of the peptide-unbound N-terminal EC domain of hPAC1-RS to investigate the structural differences that are induced by peptide binding. These results are expected to enhance the understanding of the peptide recognition mechanism and the selectivity of PAC1-R. Furthermore, since PAC1-R was discovered from rat cDNA in 1993 [8], its function and potency have attracted attention in the field of pathophysiology. For example, PAC1-R is highly expressed in the hypothalamus, the brain stem, and the limbic system [9], and is hypothesized to be associated with several diseases, such as psychiatric disorders [10], schizophrenia [11], and Alzheimer's disease [12]. Therefore, the insight about the PAC1-R structure might be lead to the discovery of several effective medicines.

2. Methods

The initial three-dimensional (3D) structure of PACAP (6'–38') and the N-terminal EC domain of the hPAC1-Rs complex (26th to 122th residues) were obtained from the Protein data bank (PDB ID: 2JOD), as determined by NMR spectroscopy [6]. The ligand-free EC domain of hPAC1-RS (26th to 119th residues) was registered as the crystal structure (PDB ID: 3N94) and included some crystal water molecules [13]. These water molecules were removed from the initial structure before minimization. The complex and ligand-free structure, in this article, are denoted as PACAP–PAC1R and ligand-free PAC1R, respectively.

MD simulations were conducted using AMBER14 program [14]. AMBER ff14SB force field [15] was used for amino acid residues. The leap module of AmberTools was used to supplement the missing heavy atoms and hydrogen atoms that were not observed in the experimental structures. The systems were solvated using the TIP3P model [16]. Sodium ions were arranged to neutralize PAC1-R. The cyclic boundary condition was applied with 8-Å margins from the protein surfaces. The cutoff distance for van der Waals interaction was set to 10 Å, and the particle mesh Ewald method was used for calculating electrostatic interactions [17]. The SHAKE algorithm was used to constrain the bond stretching of hydrogen atoms [18]. Before MD simulations, the solvent model was relaxed and the entire systems were minimized. Next, the temperature-increasing MD simulations (from 0 to 300 K) were performed for 20 ps. Finally, equilibrating MD simulations were performed using the Langevin thermostat for 80 ns under constant pressure at 300 K. The time step of all MD simulations was 2 fs.

To validate the 3D structures that were obtained by MD simulations, root mean square deviations (RMSDs) for main-chain heavy atoms were calculated along MD trajectories. The 3D structures that were obtained after temperature-increasing MD simulations were used as reference structures for the

RMSDs. To investigate the structural flexibilities of residues, root mean square fluctuations (RMSFs) for Cα atoms were calculated using 60–80 ns MD trajectories, in which average structures were used as reference structures. To identify hydrogen bond interactions between PACAP and PAC1R, 60–80 ns MD trajectories (10,000 frames) were also analyzed. For the hydrogen bond criteria, the cutoff distance between two heavy atoms was set to 3 Å and the cutoff angles between the acceptor, hydrogen, and donor atoms were set to 120º. The hydrophobic interactions were determined by measuring distance of two hydrophobic residues with a cut-off distance of 4 Å. RMSDs and RMSFs were calculated by the cpptraj module of AmberTools14. The binding free energy (ΔG_{bind}) calculation was conducted using the molecular mechanics Poisson-Boltzman surface area (MM-PBSA) python script included within the AMBER14 package. The value of the relative dielectric constant of protein was set to 2, and that of the bulk solvent was set to 80. The MM-PBSA calculation was performed using 1,000 snapshots, which were extracted with an interval of 20 ps from the last 20 ns trajectory. The *in silico* alanine scanning protocol was further performed to investigate the contribution of a specific residue to the ΔG_{bind}.

3. Results and Discussion

3.1. Structural differences between the experimental structure and optimized structure that was obtained after MD.

80-ns MD simulations were conducted for both ligand-free PAC1R and PACAP–PAC1R (Fig. 1 and 2). The MD simulations seemed to converge to equilibrium after 50–60 ns. Therefore, the 60–80 ns MD trajectories were used for the analyses in the next sections.

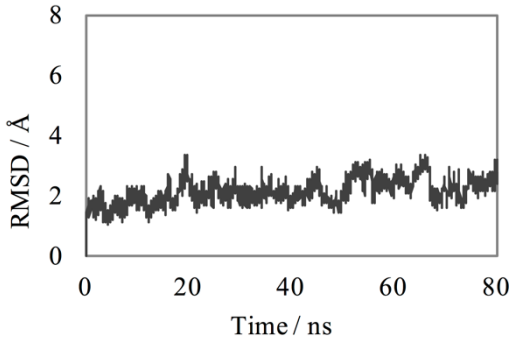

Figure 1. RMSDs for main-chain heavy atoms of ligand-free PAC1R.

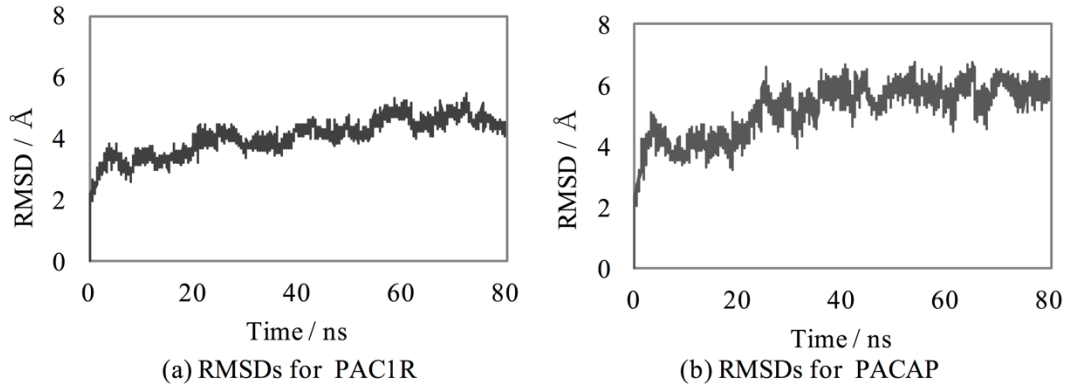

Figure 2. RMSDs for main-chain heavy atoms of PACAP–PAC1R. (a) PAC1R and (B) PACAP.

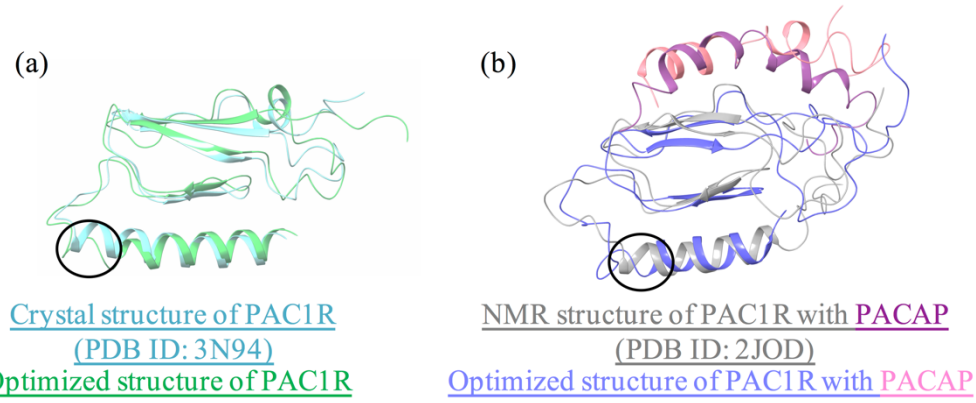

Figure 3. Superimposition of the experimental structures and optimized structures that were obtained after MD. (a) The 3N94 crystal structure of PAC1R (green) and its optimized structure (pale blue). (b) The 2JOD NMR structure of PAC1R (gray) and PACAP (violet) and the optimized structure of PAC1R (blue) and PACAP (pink). The partial loops of Arg40–Leu44 in the experimental structures are circled.

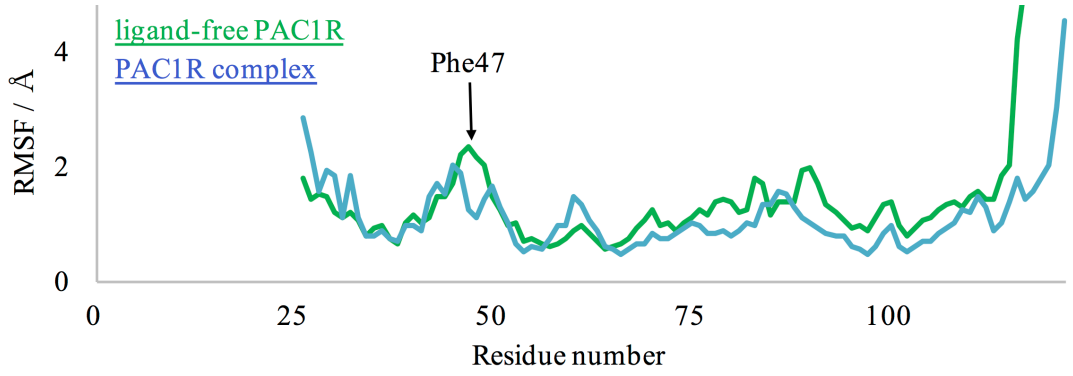

(a) Superimposition of RMSFs for PACAP–PAC1R and ligand-free PAC1R

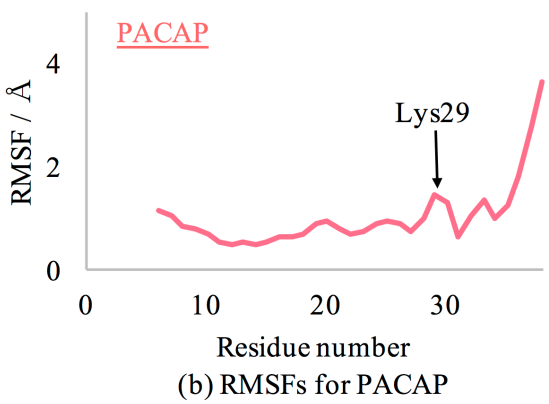

(b) RMSFs for PACAP

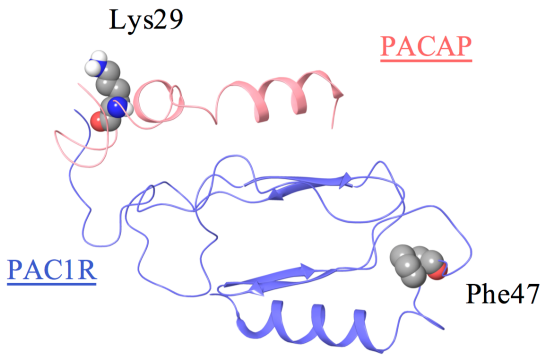

(c) Position of high RMSF peaks in PACAP–PAC1R

Figure 4. Structural flexibilities of PACAP–PAC1R and the ligand-free PAC1R. (a) Superimposed RMSFs for Cα atoms of PAC1R–PACAP (blue) and the ligand-free PAC1R (green). High RMSF peaks are indicated by arrows and residues are labeled. The RMSF values of C-terminal residues are not considered because they were exposed and not involved in the interaction with PACAP. (b) RMSF of PACAP. (c) Residues of high RMSF peaks in the PACAP–PAC1R complex.

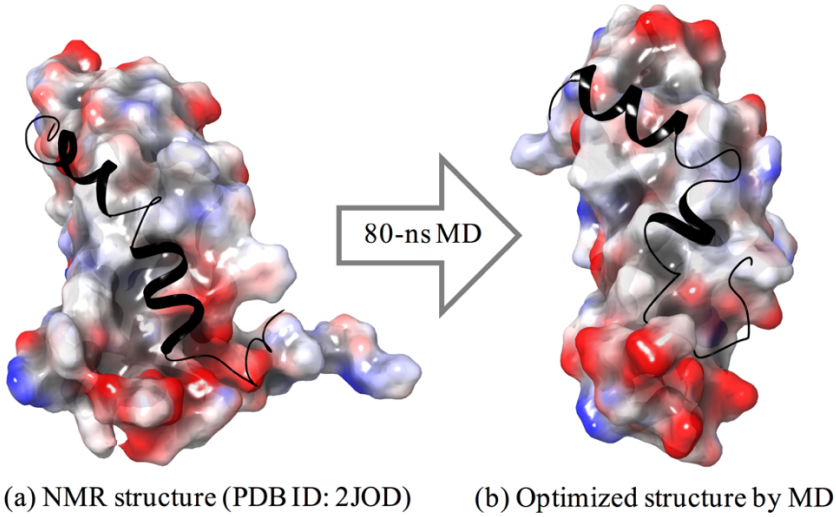

Figure 5. Molecular surfaces of PACAP–PAC1R, colored according to the electrostatic potential. (a) the NMR structure and (b) the optimized structure by MD. PACAP is shown as a black ribbon.

The RMSD values of ligand-free PAC1R converged to relatively small values of approximately 1.5 ~ 3.3 Å after 50 ns (the final RMSD: 2.60 Å), as shown in Fig. 1, which suggests that the crystal structure of ligand-free PAC1R was well retained during MD simulation. In contrast, the RMSD values of PAC1R in PACAP–PAC1 were approximately 4 Å during 60–80 ns (the final RMSD: 4.37 Å; Fig.2(a)), which is somewhat higher than that of the ligand-free PAC1R. Moreover, the RMSD values of PACAP reached almost 6 Å, though it also reached convergence after 40 ns (the final RMSD: 5.69 Å). Since PACAP is a linear peptide that is constituted by 33 residues (6'–38'), the high RMSD value of PACAP would be acceptable. It was expected that the high RMSD values of PAC1R in PACAP–PAC1R were due to the binding of the flexible PACAP.

Figures 3(a) and 3(b) show superimpositions of the initial and optimized structures of the ligand-free PAC1R and PACAP–PAC1R, respectively. Additionally, the RMSFs of their Cα atoms are shown in Figure 4. According to Fig. 3(a), although significant differences were not observed between the 3N94 crystal structure and the optimized ligand-free PAC1R, the length of the α1 helix was shortened and the residues between Arg40 to Leu44 formed a loop in the optimized structure. Likewise, a loop substructure from Arg40 to Leu44 was also observed in the optimized PACAP–PAC1R (Fig. 3(b)). In both optimized structures, the main-chain oxygen atom of Arg40 did not interact with Leu44 to form the α-helix conformation. Moreover, although the side chains of Arg40 were exposed to the solvent in both initial structures, those of Arg40 interacted with Glu36 in both optimized structures, which is why the α1 helices were partially unfolded. Moreover, in the loop that leads to the α1 helix, the highest RMSF peaks were observed in both the ligand-free PAC1R and PACAP–PAC1R (Fig, 4(a)), which suggests that these regions were originally flexible despite the PACAP binding. The RMSF peak at Phe47 was higher in the ligand-free PAC1R (2.33 Å) than in PACAP–PAC1R (1.23 Å). The RMSF differences around Phe47 were distant from the peptide binding site; thus, it might not be involved in the interaction with PACAP.

The receptor structures were similar as compared with the initial and optimized PACAP–PAC1R structures (Fig. 3(b)), except for the peptide-interacting region. Regarding the optimized PACAP structures (Fig. 3(b)), the α-helix conformation was unfolded and the C-terminal side of the peptide had moved from its initial position. Figure 5 shows the molecular surfaces of the initial and the optimized PACAP–PAC1R structures, colored with the electrostatic potential. As shown in Fig. 3(b) and Fig. 5, the peptide conformation was significantly changed by 80-ns MD and the molecular

surfaces of the receptor were also different. This result implies that both the peptide and the interaction surface of PAC1R easily fluctuated. In the peptide-binding region of the receptor (72nd to 122nd residues), the RMSFs were relatively higher in the ligand-free PAC1R structure than in PACAP–PAC1R structure, which suggests that the peptide binding stabilized the receptor structure and restricted its movement.

3.2 Comparison of the interaction between PACAP and PAC1R.
To identify the interaction between PAC1R and PACAP, hydrogen bonds that were observed in the optimized PAC1R–PACAP were compared with those of the initial structure (PDB ID: 2JOD; Fig. 6). The hydrogen bond frequencies are shown in Table 1. In the initial structure (Fig. 6(a)), five hydrogen bonds were observed, in Ser11'–Glu71, Tyr22'–Val92, Lys32'–Thr122, Lys36'–Asp24, and Arg34'–Asp24.

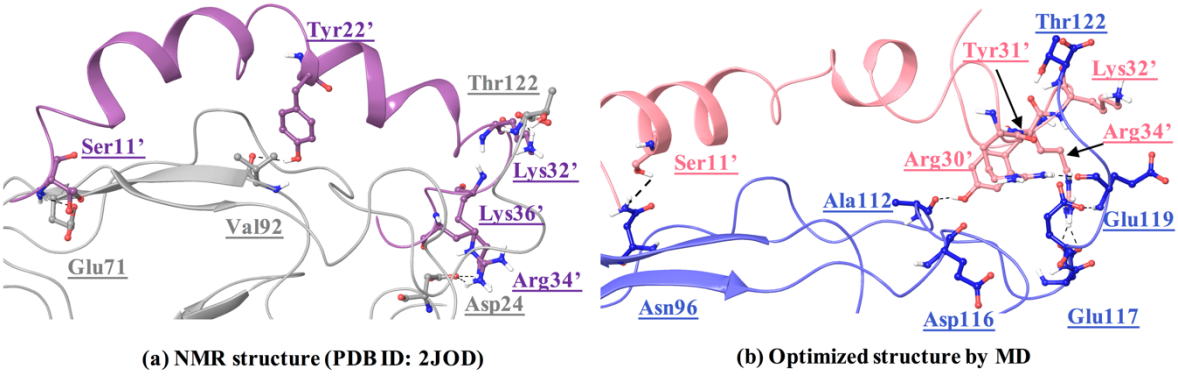

Figure 6. Hydrogen bonds between PACAP and PAC1R of (a) the initial NMR structure (PDB ID: 2JOD) and (b) the optimized structure. Hydrogen bonds > 10 % are shown as black dashed lines.

Table 1. Hydrogen bond frequencies using 60–80 ns MD trajectories of PAC1R–PACAP*

		PAC1R (26–122)						
		Glu79	Asn96	Ala112	Asp116	Glu117	Glu119	Thr122
PACAP (6'–38')	Ser11'		25.8 %					
	Gly28'							9.3 %
	Lys29'							10.0 %
	Arg30'	37.1 %					40.9 %	
	Tyr31'		4.8 %	62.8 %				
	Lys32'					42.2 %		
	Arg34'				63.2 %			

*1,000 frames were calculated and hydrogen bond frequencies of over 3 % are listed.

In contrast, in the optimized structure (Fig. 6(b)), strong hydrogen bonds (of frequency > 20 %) were formed in Ser11'–Asn96 (25.8 %), Arg30'–Glu79 (37.1 %), Arg30'–Glu119 (40.9 %), Tyr31'–Ala112 (62.8 %), Lys32'–Glu117 (42.2 %), and Arg34'–Asp116 (63.2 %). Comparing the hydrogen bonds of the optimized structure with those of the initial structure, although the hydrogen bond

patterns were not same, the basic residues of PACAP (Lys32' and Arg34') and the hydrophilic residues (Ser11' of PACAP and Thr122 of PAC1R) were equally involved in the hydrogen-bonding interaction. As shown in Table 1, the C-terminal side of PACAP has 4 basic residues (Lys29', Arg30', Lys32', and Arg34') that form strong hydrogen bonds. This result suggests that the basic residues of PACAP participate in the peptide binding and the selectivity by electrostatic interaction. According to the experimental study, the binding affinity of PAC1R for PACAP-38 is much higher than for PACAP-27 [3]. Moreover, the mutational study by Sun et al. showed that the deletion of the 29'th to 32'th residues of PACAP significantly decreased its binding affinity (inhibition constant K_i > 15,000 nM) [6]. Additionally, in their single mutational experiments, the dissociation constant K_d for PACAP (6'–38') was 350 nM, whereas those of the Lys29'Glu and Arg30'Ala mutants were 1,000 nM and 1,500 nM, respectively. Thus, our calculation result would be in agreement with those of the experimental results. Regarding the PAC1 residues, the dissociation constant K_d of wild-type PAC1R was 200 nM and that of mutant Glu117Ala was 1,050 nM, which indicate that Glu117 played an important role in the peptide-binding. It is expected that the acidic residues of PAC1R (Asp116, Glu117, and Glu119) also contribute to the peptide binding and the selectivity. In order to investigate the contribution of these polar residues on the binding affinity, we conducted binding free energy (ΔG_{bind}) calculation by MM-PBSA method and *in silico* alanine scanning protocol. In the alanine scanning, each of acidic residues of PAC1R (Asp116, Glu117, Glu119) and basic residues of PACAP (Arg30', Lys32', Arg34') was substituted by alanine because they form strong hydrogen bonds between the receptor–peptide. Moreover, in order to compare with these polar residues, each of Ser120 of PAC1R and Gln33' of PACAP, which do not form hydrogen bonds between the receptor–peptide, was also substituted by alanine. The contribution of a specific residue was estimated by a difference ($\Delta\Delta G_{bind}$) between a ΔG_{bind} value of the mutated complex, in which the specific residue was replaced by alanine, and that of the wild-type complex. The results are shown in Table 2. As expected, we could see that the contribution of Ser120 of PAC1R and Gln33' of PACAP were quite small, because the $\Delta\Delta G_{bind}$ values were estimated to be 0.25 and 0.50 kcal/mol, respectively. By contrast, regarding polar residues forming hydrogen bonds, $\Delta\Delta G_{bind}$ values were estimated to be much greater. For example, the $\Delta\Delta G_{bind}$ value of 12.49 kcal/mol was obtained for the R30'A mutant of PACAP. These results indicate that the polar residues forming strong hydrogen bonds have significant contribution on the binding affinity of the PAC1R–PACAP.

Table 2. Differences of binding free energies between mutated complex and wild-type complex*[1,2]

Alanine mutant	PAC1R				PACAP			
	D116A	E117A	E119A	S120A	R30'A	K32'A	Q33'A	R34'A
$\Delta\Delta G_{bind}$ (kcal/mol)	6.75 (1.85)	10.73 (4.12)	3.79 (1.15)	0.25 (0.41)	12.49 (4.11)	8.34 (4.89)	0.50 (1.48)	7.81 (2.22)

*1 mean values using 1,000 frames extracted with an interval of 20 ps from 60-80 ns. Values in parenthesis were standard deviations.
*2 $\Delta\Delta G_{bind}$ no more than 0.5 kcal/mol were shadowed.

Figure 7 shows the hydrophobic interaction between PACAP and PAC1R. In the optimized structure, Tyr10' was located near Met72 and Ala112. Moreover, Tyr22', Val26', and Leu27' interacted with Pro107, Leu74, and Leu80. These hydrophobic residues, except for Leu80 and Ala112, were substituted by alanine scanning and the binding constants of the alanine mutants were investigated [6]. For alanine mutation on PACAP, the values of the inhibition constant Ki for Y10'A, Y22'A, V26'A, and L27'A were 670 nM, > 15,000 nM, > 15,000 nM, and 6,800 nM, respectively (Ki of the wild-type: 350 nM). In contrast, for the alanine mutants of PAC1R, the values of the

dissociation constant Kd for M72A, L74A, and P107A were 440 nM, 580 nM, and 840 nM, respectively (Kd of the wild-type: 200 nM). Thus, these hydrophobic interactions between PACAP and PAC1R also contribute greatly to the peptide binding.

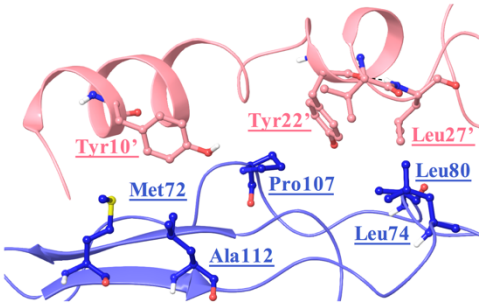

Figure 7. Hydrophobic interaction between PACAP and PAC1R of the optimized structure.

4. Conclusion

In this study, we investigated the interaction between the N-terminal EC domain of PAC1R and the potent antagonist PACAP (6'–38'). Strong hydrogen bonds were observed between the basic residues of PACAP (Arg30', Lys32', Arg34') and the acidic residues of PAC1R (Asp116, Glu117, Glu119). These residues would be important for peptide binding and ligand selectivity. Moreover, Met72, Leu74, Leu80, Pro107, and Ala112 of PAC1R and Tyr10', Tyr22', Val26', and Leu27' of PAC1R also contribute to peptide binding. Our results would be informative for developing a selective PAC1-R inhibitor.

References

[1] Merskey H and Bogduk N 1994 *Classification of Chronic pain* 2nd ed, Merskey H and Bogduk N (Seattle: IASP Press) pp 209–14
[2] Dickinson T and Fleetwood-Walker SM 1999 VIP and PACAP: very important in pain? *Trends Pharmacol. Sci.* **20** 324–9
[3] Laburthe M and Couvineau A 2002 Molecular pharmacology and structure of VPAC Receptors for VIP and PACAP *Regul. Pept.* **108** 165–73
[4] Rosenbaum DM, Rasmussen SG and Kobilka BK 2009 The structure and function of G-protein-coupled receptors *Nature* **459** 356–63
[5] Dickinson T, Fleetwood-Walker SM, Mitchell R and Lutz EM 1997 Evidence for roles of vasoactive intestinal polypeptide (VIP) and pituitary adenylate cyclase activating polypeptide (PACAP) receptors in modulating the responses of rat dorsal horn neurons to sensory inputs *Neuropeptides* **31** 175–85
[6] Sun C, Song D, Davis-Taber RA, Barrett LW, Scott VE, Richardson PL, Pereda-Lopez A, Uchic ME, Solomon LR, Lake MR, Walter KA, Hajduk PJ and Olejniczak ET 2007 Solution structure and mutational analysis of pituitary adenylate cyclase-activating polypeptide binding to the extracellular domain of PAC1-RS *Proc. Natl. Acad. Sci. USA* **104** 7875–80
[7] De Vivo M, Masetti M, Bottegoni G, Cavalli A 2016 Role of molecular dynamics and related methods in drug discovery *J. Med. Chem.* **59** 4035-61
[8] Hashimoto H, Ishihara T, Shigemoto R, Mori K and Nagata S 1993 Molecular cloning and tissue distribution of a receptor for pituitary adenylate cyclase-activating polypeptide *Neuron* **11** 333–42
[9] Otto C, Zuschrattera W, Gass P and Schützb G 1999 Presynaptic localization of the PACAP-typeI-receptor in hippocampal and cerebellar mossy fibres *Mol. Brain Res.* **66** 163–74
[10] Hashimoto H, Shintani N, Tanida M, Hayata A, Hashimoto R and Baba A 2011 PACAP is implicated in the stress axes *Curr. Pharm. Des.* **17** 985–89

[11] Hashimoto R, Hashimoto H, Shintani N, Chiba S, Hattori S, Okada T, Nakajima M, Tanaka K, Kawagishi N, Nemoto K, Mori T, Ohnishi T, Noguchi H, Hori H, Suzuki T, Iwata N, Ozaki N, Nakabayashi T, Saitoh O, Kosuga A, Tatsumi M, Kamijima K, Weinberger DR, Kunugi H and Baba A 2007 Pituitary adenylate cyclase-activating polypeptide is associated with schizophrenia *Mol. Psychiatry* **12** 1026–32

[12] Rat D, Schmitt U, Tippmann F, Dewachter I, Theunis C, Wieczerzak E, Postina R, van Leuven F, Fahrenholz F and Kojro E 2011 Neuropeptide pituitary adenylate cyclase-activating polypeptide (PACAP) slows down Alzheimer's disease-like pathology in amyloid precursor protein-transgenic mice *FASEB J.* **25** 3208–18

[13] Kumar S, Pioszak A, Zhang C, Swaminathan K and Xu HE 2011 Crystal structure of the PAC1R extracellular domain unifies a consensus fold for hormone recognition by class B G-protein coupled receptors *PLoS One* **6** e19682

[14] Case DA, Babin V, Berryman JT, Betz RM, Cai Q, Cerutti DS, Cheatham TE III, Darden TA, Duke RE, Gohlke H, Goetz AW, Gusarov S, Homeyer N, Janowski P, Kaus J, Kolossváry I, Kovalenko A, Lee TS, LeGrand S, Luchko T, Luo R, Madej B, Merz KM, Paesani F, Roe DR, Roitberg A, Sagui C, Salomon-Ferrer R, Seabra G, Simmerling CL, Smith W, Swails J, Walker RC, Wang J, Wolf RM, Wu X and Kollman PA 2014 *AMBER 14* University of California, San Francisco.

[15] Maier JA, Martinez C, Kasavajhala K, Wickstrom L, Hauser KE and Simmerling C 2015 ff14SB: Improving the accuracy of protein side chain and backbone parameters from ff99SB *J. Chem. Theor. Comput.* **11** 3696–713

[16] Joung IS and Cheatham TE III 2008 Determination of alkali and halide monovalent ion parameters for use in explicitly solvated biomolecular simulations *J. Phys. Chem. B* **112** 9020–41

[17] Darden TA, York DM and Pedersen LG 1993 Particle mesh Ewald: An N·log(N) method for Ewald sums in large systems *J. Chem. Phys.* **98** 10089–92

[18] Ryckaert JP, Ciccotti G and Berendsen HJC 1977 Numerical integration of the cartesian equations of motion of a system with constraints: molecular dynamics of n-alkanes *J. Comput. Phys.* **23** 327–41